Arabian Journal of Chemistry (2023) **16**, 104714

King Saud University

Arabian Journal of Chemistry

www.ksu.edu.sa
www.sciencedirect.com

ORIGINAL ARTICLE

The selective and enhanced adsorptive behaviors of supramolecular recrystallized 1,3,5-benzenetricarboxylic acid assembled nano-bacterial cellulose

Zengbei Li [a], Xin Huang [a,b,c,*], Haijuan Du [a,b,*], Xinjie Deng [a], Chaoyang Deng [a], Shaobo Wang [a,b,*], Xianyang Yue [a,b], Xiaozhou Su [a,b]

[a] *Department of Light Chemical Engineering, College of Textiles, Zhongyuan University of Technology, No. 41 Zhongyuan Road (M), Zhengzhou, Henan Province 450007, China*
[b] *Collaborative Innovation Centre of Advanced Textile Equipment and Technology Co-constructed by Ministry of Education and Henan provincial Government, Zhengzhou, Henan Province 451191, China*
[c] *Zhengzhou Key Laboratory of Green Dyeing and Finishing Technology, Zhengzhou, Henan Province 451191, China*

Received 13 December 2022; accepted 20 February 2023
Available online 25 February 2023

KEYWORDS

Nano-bacterial cellulose;
Supramolecular hexamer;
Cationic dyes;
Distinct adsorption behaviors;
High efficiency

Abstract The effluent discharge produced in the textile printing and dyeing, leather and other fields, will cause the irreversible environmental pollution and extremely threatening safety of living organisms. The appropriate and efficient disposal method of dyestuff originated wastewater has been widely concerned in the past decades. In this study, the recrystallization of 1,3,5-benzene tricarboxylic acid (RCTMA) was put forward *via* a hydrothermal method to form the supramolecular RCTMA-based hexamer and thereafter assembled into the porous nano-bacterial cellulose (NBC) to construct the RCTMA@NBC composite. The morphology and surface properties of RCTMA@NBC were examined by scanning electron microscope, X-ray diffraction, and Fourier transform infrared spectroscopy. This RCTMA@NBC was employed to adsorb methylene blue (MB) adjusting the pH, temperature, and dosage of adsorbent. The result showed the maximal absorption capacity of RCTMA@NBC appeared under pH = 7.1 and higher temperature will hinder the adsorption of dyes. Moreover, the adsorption isotherms and kinetics were evaluated which was more confirmed to Langmuir model and quasi-second-order kinetic equation, and the simulated maximum adsorp-

* Corresponding authors at: Department of Light Chemical Engineering, College of Textiles, Zhongyuan University of Technology, No. 41 Zhongyuan Road (M), Zhengzhou, Henan Province 450007, China.
E-mail addresses: xinhuang@zut.edu.cn (X. Huang), duhaijuan2009@126.com (H. Du), shaobowang@zut.edu.cn (S. Wang).
Peer review under responsibility of King Saud University.

Production and hosting by Elsevier

https://doi.org/10.1016/j.arabjc.2023.104714

tion capacities of MB was 1162.12 mg/g. Moreover, cationic golden XGL and anionic brilliant crocein were selected to further verify the distinct adsorptive behavior. The excellent affinity towards cationic dyes proved the easy combination was based on the chemical force originated from mutual attraction between opposite charges, π–π interactions, and H-bonding, whereas the poor attraction for brilliant crocein was due to the electrostatic repulsion between sulfonic and carboxyl groups. The synthesized RCTMA@NBC possesses higher efficiency and selective adsorption, which exhibits the promising potential in the field of precise treatment of organic dye wastewater.

1. Introduction

Organic dyes with stable molecular structure and delightful optical property are frequently used in textile printing and dyeing, food, fine organic chemistry, leather and other economic fields. (Han et al., 2021; Samsami et al., 2020) Excessive dyes which are directly discharged into the water environment will cause severe environmental pollution and pose effects like large chemical oxygen demand (COD) and biochemical oxygen demand (BOD), complex chemical composition, toxicity to ecosystem. (Nidheesh et al., 2018) More seriously, the majority of organic dyes are sensitized and carcinogenic which could cause the dysfunction of liver, kidney and central nervous system. (Ali, 2012) Considering the inevitable effluent discharge accompanied by the production process, appropriate and efficient disposal method of dyestuff wastewater should be widely concerned. The treatment methodologies of dye wastewater mainly contain physical treatment, chemical method and biological treatment process. Despite their own advantages and certain application fields, chemical methods like advanced oxidation processes (AOPs) and electrochemical treatment, have the non-ignorable drawbacks including high cost of oxidants, strict technological conditions, and high energy consumption. Similarly, biological treatment process including microbiological degradation should address the problem like long treatment cycle, and unstable treatment efficiency. Thus, physical treatment such as membrane separation, flocculation, especially adsorption, (Qiu et al., 2022) is still the mainstream method solving the pollution of industrial wastewater due to its advantage of low cost, convenient operation and low energy consumption. The mature adsorption technology has been already used for centralized process of wastewater and the common adsorbents are activated carbon, (Rivera-Utrilla et al., 2011) zeolite, (Wang and Peng, 2010) graphenes, (Yan et al., 2019; Du et al., 2015; Yan et al., 2019; Du et al., 2015; Hirani et al., 2022) magnetic composites, (Chang et al., 2020; Du et al., 2022; Cao et al., 2023) metal–organic frameworks (MOFs), (Uddin et al., 2021; Tang and Yamauchi, 2016; Wang et al., 2020) covalent organic frameworks (COFs), (Xia et al., 2021) which mainly depend on the porous adsorption, magnetic separation, electrostatic interaction, π–π or H-bonding interaction to realize the adsorption separation of organic dyes in effluent. Nowadays, developing a precisely-selected, environmentally-friendly, and low-cost adsorbent has gradually became a promising candidate for cost-effective and sustainable water purification.

Nanocellulose (NC) including cellulose nanofibrils (CNF), cellulose nanocrystals (CNC), tunicate cellulose nanocrystals (*t*-CNC), nanobacterial cellulose (NBC) and algae cellulose particles (Das et al., 2022) was extracted from abundant and accessible plant biomass and incrementally applied in the wastewater treatment for the past decades. NBC as a renewable bio-material produced by bacterial fermentation, has biodegradability characteristics, good biocompatibility, high crystallinity, ultra-fine three-dimensional network structure and hydrophilicity. (Cazón and Vázquez, 2021) As an adsorbent material, NBC still exist the disadvantages of poor specificity and low adsorption capacity. In order to address this problem, NBC was often compounded with ionic polymer, surfactant, and microporous or mesoporous materials to endow its functionality. Huang *et al.* (Huang et al., 2020) reported that the polyethylenimine caged platinum nanomaterials modified NBC (defined as PEI-Pt@NBC) produced by a facile in-situ reduction method not only significantly increased the adsorption capacity of NBC but also provided the substrate for PEI-Pt. PEI-Pt in-situ synthesized onto NBC was beneficial to the recovery and reuse after adsorption. Yin's group (Yin et al., 2012) put forward a 2D MOF coating on NBC with (3-aminopropyl)triethoxysilane and hyaluronic acid as surface modification agent of NBC to ensure strong binding between MOF and NBC. Accordingly, the preparation of BC and MOF composite materials is particularly useful in solving the difficult recovery of MOF powders. In addition, hydrogen bonding plays a vital role in the areas of chemistry, such as supramolecular chemistry, crystal engineering and material. Benzene carboxylic acids served as an archetypal example of hydrogen bonded systems, which makes 1,3,5-benzene tricarboxylic acid (trimesic acid, TMA) as a polycarboxyl compound receive extensive attention. (Rajkumar et al., 2020) The carboxylic groups of TMA can form cyclic dimer and trimeric associations through hydrogen-bonding. Jos'e Elías Conde-Gonzalez *et al.* (Conde-González et al., 2021) synthesized nanoporous Fe-(1,3,5-tricarboxylic acid) metal–organic framework to absorb fluorescent anionic dyes from the aqueous solution. Adsorption capacity of the adsorbent for 2′,4′,5′,7′-tetra-bromofluorescein sodium salt was reached at 0.836 mg/g. Liu' group reported an organic metal skeleton material with Cu as the metal centre and H_3BTC as the ligand to form $Cu_3(BTC)_2$, which had good adsorption for Th(IV) with a maximum adsorption of 757.58 mg/g. (Hu et al., 2020) Similarly, high crystallinity $Cu_3(BTC)_2$ modified by agarose (AG) exhibited a maximum adsorption capacities of MB at 282.466 mg/g *via* the formation of a monolayer adsorption onto the homogeneous surface of Cu-BTC@AG. (Fu et al., 2022).

Herein, we proposed a simple preparation of supramolecular recrystallized TMA (RCTMA) and subsequently assembling into the three-dimensional network NBC to form RCTMA@NBC membrane *via* simple freeze-drying method. Scanning electron microscope (SEM), X-ray diffraction (XRD), Fourier transform infrared spectroscopy (FTIR) were used to determine the morphology and structure of resultant RCTMA@NBC composite membrane and proved that RCTMA could anchor into NBC nanofibers which still maintain the porous morphology. The effects of time, temperature, adsorption dose, and pH on adsorption were investigated. Thereafter, the distinguish adsorption behaviors of RCTMA@NBC were studied through kinetics and thermodynamics. These results indicate that RCTMA@NBC had a preferential adsorption ability of cationic organic dye than anionic dye. RCTMA@NBC revealed the advantage of highly efficient, simple operation and recovered easily, and has a broad prospect in the treatment of dye wastewater.

2. Materials and methods

2.1. Materials

All chemicals used were analytical grade and without any further purification. NBC hydrogel (water content = 25 %, diameter = 50–100 nm and length = 20 μm) was brought

from Guilin Qihong Technology Co., ltd. of China. Brilliant crocein, cationic gold yellow XGL were all purchased from Hebei Changlu Chemical Dye Co., ltd. Methylene blue (MB) was purchased from Tianjin Kemiou Chemical Reagent Co., ltd. H_3TMA (99.9 %), hydrochloric acid (HCl, 36.0–38.0 %), ethanol absolute (99.7 %), sodium hydroxide (NaOH, 99.0 %), spectrum pure potassium bromide (KBr, 99.9 %) were purchased from National Medicines Corporation ltd. of China. The ultra-pure water used throughout all experiments was purified by a UPD0-P-500 ultrapure water purification system (Youpu Co., ltd., China) and the air was removed by N_2 over 0.5 h.

2.2. Recrystallization of H_3TMA

An aqueous mixture of H_3TMA (0.5 mM, 0.1050 g) and minimum quantities of $Zn(NO_3)_2{\cdot}6H_2O$ were dissolved in water (15 mL) under stirring for 0.5 h at room temperature. Then they were placed in a stainless steel vessel, which was sealed and placed in a programmable oven. They were heated at 120 °C for 14 h then cooled at 10 °C/min to room temperature. The large prismatic crystals were obtained, namely RCTMA.

2.3. X-ray crystallography study

Crystallographic data for the RCTMA were collected at 100(2) K on a Bruker APEX-II area-detector diffractometer equipped with graphite-monochromatized Mo-Kα radiation (λ = 0.71 073 Å). Their structures were solved by direct method and expanded using Fourier techniques. The non-hydrogen atoms were refined with anisotropic thermal parameters. The hydrogen atoms were assigned with common isotropic displacement factors and included in the final refinement by using geometrical constraint. The structures were refined with full-matrix least-squares techniques on F^2 using the OLEX-2 program package. Crystal data for RCTMA were summarized in detail in Table S1 (SM-1).

2.4. Synthetic process of RCTMA@NBC

NBC hydrogel was used as the matrix and mixed the RCTMA (0.375 mg) into NBC (25 g) adequately to synthesis of RCTMA@NBC under the constant stirring for 4 h. The mixture of the RCTMA@NBC was formed a film shape by a freezer dryer (scientz-10ND, Ningbo Scientz Biotechnology Co., ltd.) for 12 h. After the carefully washing and drying again, the RCTMA@NBC was then applied to treatment of the cationic dyes containing effluent.

2.5. Adsorption experiments

The adsorption experiments were conducted with the RCTMA@NBC composite membrane (180 mg) as the adsorbent for MB dyes (180 mL, 100 mg/L) in a beaker, adjusting the factors of pH, temperatures and dosage of adsorbent. The pH of the staining solution was changed from 1 to 12 by changing the amount of NaOH (0.1 M) and HCl (0.1 M). The adsorption experiment was put forward under the temperature at 298 K and the rotation speed of 300 r/min. The effect of temperature on adsorption ability was carried out under the rotation speed of 300 r/min and the different temperatures at 298 K, 313 K, 333 K, respectively. The obtained supernatant was centrifuged for 5 min (13500 × g). The dosage of RCTMA@NBC from 50 − 400 mg per 180 mL sample was set to do the experiment under the pH at 7.1 and the temperature at 298 K. The adsorption capacity at different time q_t (mg/g), the equilibrium capacity q_e (mg/g) and dye removal efficiency r (%) are calculated using the following equations:

$$q_t = \frac{(C_0 - C_t) \times V}{m} \tag{1}$$

$$q_e = \frac{(C_0 - C_e) \times V}{m} \tag{2}$$

$$r = \frac{C_0 - C_e}{C_0} \times 100\% \tag{3}$$

where C_0 (mg/L) is the initial concentration of dyes in the solution, C_t (mg/L) is the concentration of dyes at variational times. V (L) stands for the volume of solution and m (mg) is the weight of RCTMA@NBC adsorbent. The adsorption isotherm experiment was put forward changing the concentration of MB dyes solution from 150 −1000 mg/L and the usage of RCTMA@NBC is 50 mg per 50 mL sample. Moreover, The adsorption kinetics experiment was carried using 180 mg RCTMA@NBC to absorb the MB aqueous solution (180 mL, 1000 mg/L) under the varied time intervals, up to 8 h. The same adsorption isotherm experiment of cationic golden XGL and anionic brilliant crocein was carried out as same as that of MB.

2.6. Characterization

SEM (Zeiss Gemini 300, German) was used to determine the porous morphology of TMA@NBC membrane at 3.00 kV and the test samples were treated by spray-gold before the measurement. XRD (Rigaku Ultima IV) was used to detect the RCTMA@NBC membrane. pH was recorded by Precision pH meter (PHS-3C, Hangzhou aurilong instrument Co., ltd., China). UV–*vis* and FTIR data were tested by Agilent Cary 5000 Spectrometer (Agilent Technologies, Inc., USA) under the wavelength of MB, cationic golden XGL and anionic brilliant crocein at 664 nm, 438 nm, and 503 nm, respectively. FTIR data were examined by Thermo Nicolet Nexus-870 FTIR Spectrometer (Thermo Fisher Scientific Inc., USA) using the KBr pellet method.

3. Results and discussion

3.1. Synthesis and characterization of RCTMA@NBC membrane

Crystal structures of RCTMA. Supramolecular RCTMA was prepared from the recrystallization of H_3TMA *via* a hydrothermal method. The single crystal X-ray diffraction analysis showed that large prismatic crystal was crystallized in the monoclinic space group *C*2/*c*. In the Fig. 1a, it can be seen that the asymmetric unit contained six molecules of trimesic acid. Linking neighbouring trimetric acids TMA resulted in planar ribbons with hydrogen bonds together through their COOH groups along the b-axis. (Duchamp and Marsh,

1969) These rings are further connected to form a two-dimensional (2D) parallelogram network viewing from the *ac* plane. (Fig. 1b). Thus, a supramolecular structure of hexamer could be constructed from the small molecular TMA *via* the hydrogen bonding.

Synthesis and Characterization of RCTMA@NBC. The RCTMA@NBC was synthesized by effortlessly assembling the RCTMA into porous NBC (Fig. 2a, and Fig. S1). The geometrical shape and surface morphology of RCTMA@NBC was determined by SEM technique. As can be seen in Fig. 3a, NBC materials possess three-dimensional (3D) interlaced porous networks with the average diameter around 40 ± 20 nm. After then formation of RCTMA@NBC, crystalline bulk RCTMA was embedded into the network of nanofibers and the NBC still maintain the loose and reticulate structure (Fig. 3b). Fig. 3c shows the XRD diffraction patterns of NBC and RCTMA@NBC. The positions at 11°, 12°, 13°, 24.5°, 27.9°, 30°, 31.2°, 32.4° are correspond to diffraction peaks of RCTMA. (Yaghi et al., 1996) The broad peaks at 14.6°; 16.8° and 22.8° appear in the pattern of RCTMA@NBC, which are assigned to the typical peaks of crystallographic plane ($1\bar{1}0$), (110) and (200) from the reflection of NBC. (Tokoh et al., 1998).

Subsequently, FTIR spectra was used to determine the characteristic peak of functional group. Fig. 3d shows that the characteristic peaks of BC at 3337 cm^{-1} and 2893 cm^{-1} are ascribed to stretching vibration of O—H and C—H, respectively. Meanwhile, the peaks at 1160, 1110, and 1060 cm^{-1} are assigned to the glycosidic link of C1-O-C4, C3-O3, C6-O6, respectively. (Lv et al., 2017) As for RCTMA, the peak at 3089 cm^{-1}, 1714 cm^{-1}, 1608 cm^{-1}, and 1275 cm^{-1} represent the stretching of O—H, C═O, C—O in carboxyl group. The deformation of O—H exhibits at 1455, 1400, 924 cm^{-1}. Obviously, the characteristic peaks of both NBC and RCTMA can be found in the FTIR spectra of RCTMA@NBC. Based on these results shown above, RCTMA has been successfully self-assembled into the NBC matrix and constitute an intertwined composite morphology.

3.2. Adsorption performance for cationic dyes

Based on the introduction of plentiful carboxyl group onto the NBC, the effect of pH, temperature, and adsorbent dosage on absorption behaviors of RCTMA@NBC was estimated, choosing the cationic dyes MB as the target dye (Fig. 2b).

3.2.1. Effect of pH on adsorption performance for cationic dyes

The solution pH was the key factor influencing the adsorption performance, (Dou et al., 2023) thus the effect of initial solution pH on adsorption performance were put forward to evaluate the adsorption capacity of RCTMA@NBC. As shown in Fig. 4a, the q_e of RCTMA@NBC is 79.41 mg/g when the pH was 2.1. The carboxyl functional groups are mostly in the non-ionized form under the strong acid environment, and many H^+ in the solution can compete with dyes, resulting in weaker adsorption capacity. As the increasing of pH, the value obviously arises to over 90 mg/g. The maximal absorption capacity of RCTMA@NBC reaches to 96.72 mg/g under the neutral environment (pH = 7.1) due to the electrostatic force between the ionized carboxyl functional groups (–COO^-) of RCTMA and -C═N^+ of MB dyes, which makes MB molecule is easily absorbed. (Zou et al., 2019) Continuously increasing the pH of the solution to 9.03, the adsorption capacity of MB is slightly reduced again. The reason is possibly due to the enhanced numbers of OH^- in solution under the alkaline environment, which has an inhibiting effect on the ionization of carboxyl functional groups. (Huang et al., 2021) Obviously, the pH of solution is essential in adsorption ability of RCTMA@NBC because the number of binding sites on the adsorbent was pH-dependently influenced. Hence, the RCTMA@NBC adsorbent shows the optimal adsorption capacity under neutral conditions.

3.2.2. Effect of temperature on adsorption performance for cationic dyes

The effect of temperature on adsorption performance was also put forward setting three temperatures at 298 K, 313 K and 333 K, respectively. It can be seen in Fig. 4b, the values of adsorption capacity at three different temperatures are approximate within 5 min. As the extension of time, the differentiation becomes generally remarkable. In 298 K experimental group, the adsorption reaches an equilibrium at the 240 min, and this value is 3.5 multiples and 11.3 multiples higher than that obtained at 313 K and 333 K, respectively. The adsorption capacity rises slowly in 300 min and goes up to near 74.34 mg/g under the condition of temperature at 313 K. As for the 333 K experimental group, the data do not show any changes and maintain around 10 mg/g even the contacting time prolongs to 480 min. The equilibrium adsorption capacity of RCTMA@NBC for MB was clearly decreasing as the temperature increased, indicating high tem-

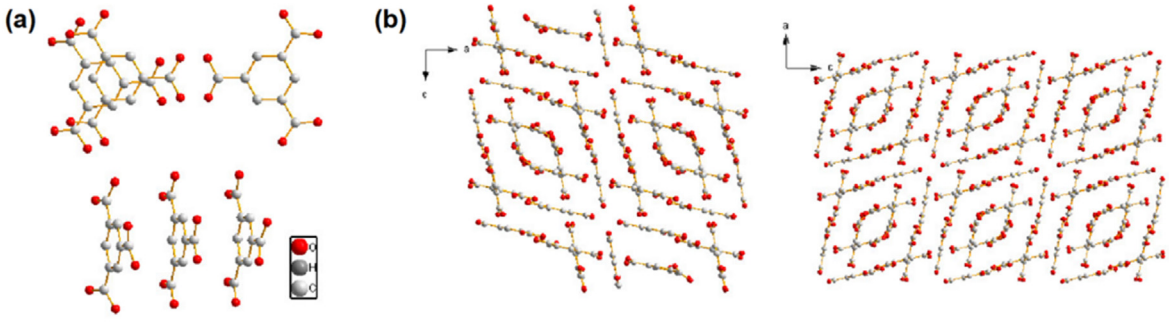

Fig. 1 (a) Supramolecular structure of recrystallized 1,3,5-benzenetricarboxylic acid (RCTMA). (b) A schematic representation of the RCTMA structure viewed down the b axis.

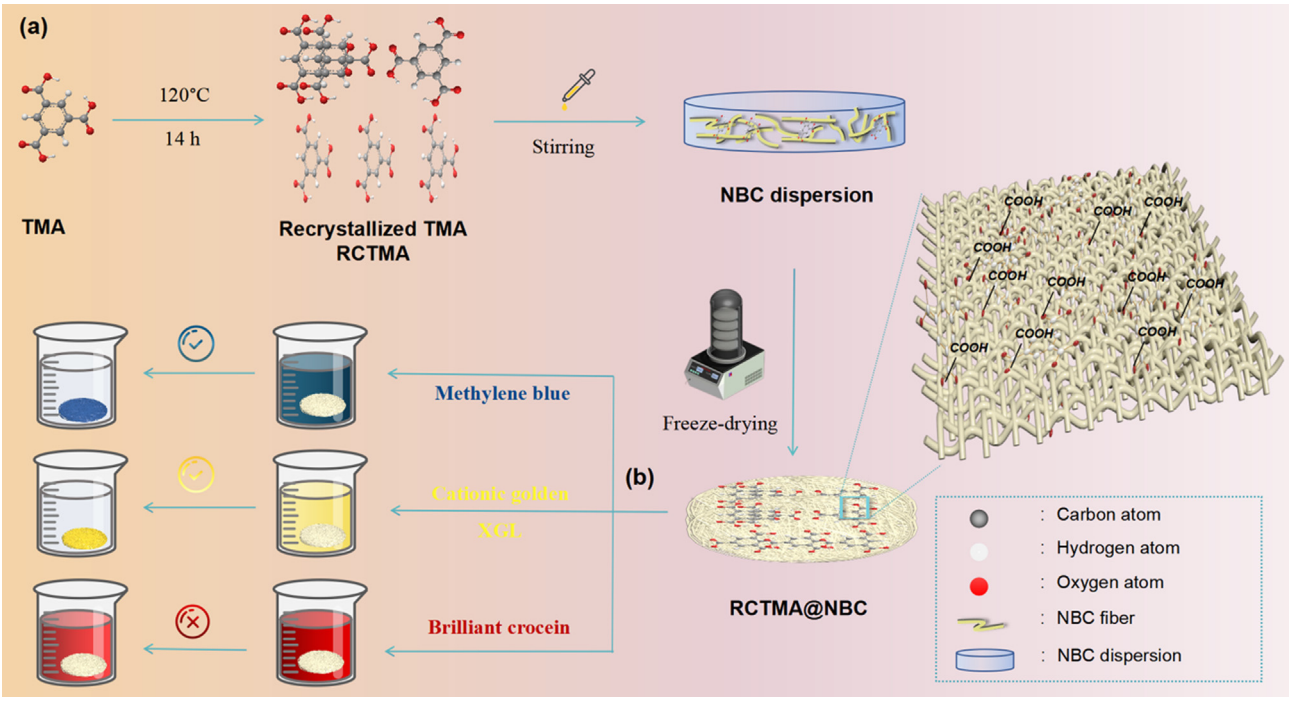

Fig. 2 (a) Schematic illustration for preparation of RCTMA@NBC and (b) their adsorption behaviors of different organic dyes.

perature is not conducive to adsorption. Overall, the adsorption capacity at 298 K is superior to other temperature control groups and low temperature is more conducive to adsorb the MB dyes for RCTMA@NBC.

Furthermore, the adsorption thermodynamics of MB by RCTMA@NBC were studied and thermodynamic parameters were acquired from the adsorption experiments at different temperatures (293, 303 and 313 K) and the initial MB concentration of 100 mg/L, following the equations 4-6 as below.

$$K_C = \frac{q_e}{C_e} \tag{4}$$

$$\ln K_C = \frac{\Delta S}{R} - \frac{\Delta H}{RT} \tag{5}$$

$$\Delta G = \Delta H - T\Delta S \tag{6}$$

where, K_C is the standard thermodynamic equilibrium constant. T (K) is the Kelvin temperature. R (8.314 J/mol/K) is the ideal gas state constant. $\triangle H$ (kJ/mol) is the enthalpy change, $\triangle$S (kJ/mol/K) is the entropy change, and $\triangle G$ (kJ/-mol) is the free energy change.

The thermodynamic fitting diagram of adsorption of MB by RCTMA@NBC is shown in Fig. S2 and Table S2 summarizes the thermodynamic parameters of MB adsorption. The negative value of $\triangle G$ (-7.2505 to −0.0580 kJ/mol) implies that the adsorption process is spontaneous at the experimental temperature (298 to 333 K). Moreover, the negative value of $\triangle H$ reveals that the adsorption is exothermic, which is consistent with the experimental results that the q_e decreases with increasing temperature. The $\triangle S$ is negative, indicating that the randomness of the solid–liquid interface decreases. In other words, when MB is adsorbed on RCTMA@NBC surface, the mobility of MB molecules on the absorbent surface is more limited than that in an aqueous solution. Therefore, the driving force of adsorption of MB by RCTMA@NBC is enthalpy change, not entropy change.

3.2.3. Effect of adsorbent dosage on adsorption performance for cationic dyes

The influence of adsorbent dosage on adsorption performance of RCTMA@NBC was evaluated by relationship between q_e, removal rate (r) and the adsorbent dosage ranged from 50 to 400 mg per 180 mL sample. Fig. 5a illustrates that the value of q_e decreases with the adsorbent dosage increasing fixing the concentration of MB solution is constant. On the other hand, removal rate of MB dyes promote as the adsorbent dosage raised and the maximum is close to 99 %. These results are due to the adsorption sites on NBC aggrandize which can adsorb more MB dyes with the absorbent dosage increasing.

3.3. Adsorption isotherms for cationic dyes

In order to examine the adsorption isotherms of RCTMA@NBC, the different concentrations of MB dyes solutions from 100 to 1000 mg/L were prepared as the simulated adsorption environment. It is evident that q_e is ascending accompanied with the increasing MB's concentration (Fig. 5b). The common four kinds of isotherms model, namely Langmuir (which is dependent on the monolayer adsorption on homogeneous sites, Equation 7), Freundlich (which is related to heterogeneous system with non-uniform heat of sorption distribution, Equation 8), Dubnin-Radushkevich (D-R) (which possibly determines the type of adsorption as chemical or physical, Equation 9) and Temkin models (which is used when the adsorbate will occur the interaction for each other during the adsorbing process, Equation 10) were described as follows to examine the adsorption isotherms of MB using the RCTMA@NBC. (Xie et al., 2021)

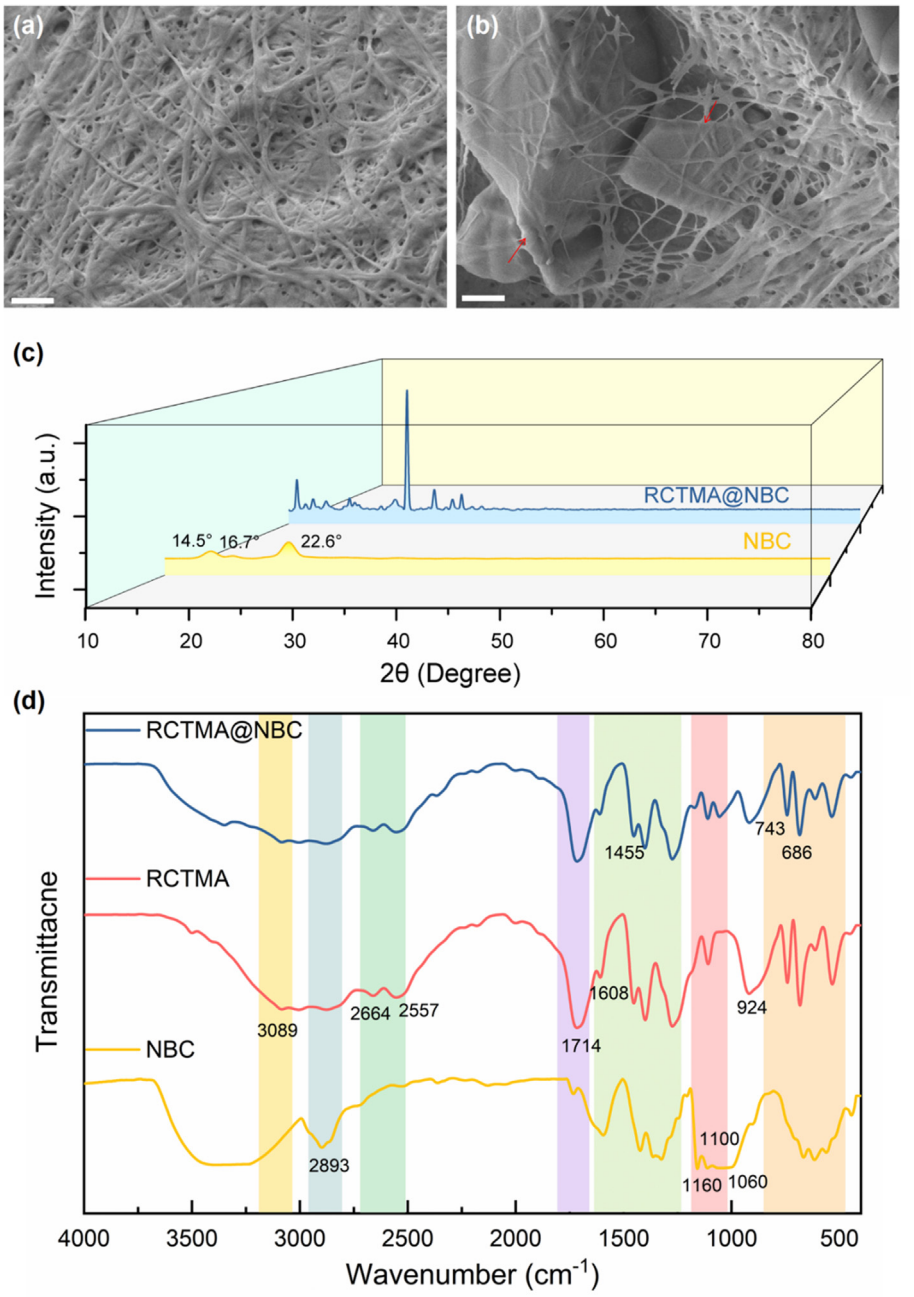

Fig. 3 SEM photographs of (a) pure NBC and (b) RCTMA@NBC. (c) XRD spectrum of pure NBC and RCTMA@NBC. (d) FTIR spectra of NBC, RCTMA and RCTMA@NBC, respectively.

$$\frac{C_e}{q_e} = \frac{C_e}{q_m} + \frac{1}{k_L q_m} \tag{7}$$

$$\ln q_e = \ln k_F + \frac{1}{n} \ln C_e \tag{8}$$

$$\ln q_e = \ln q_{D\text{-}R} - k_{D-R}\varepsilon^2 \tag{9}$$

$$q_e = \frac{RT \ln A_T}{b_T} + \frac{RT \ln C_e}{b_T} \tag{10}$$

q_e (mg/g) and q_m (mg/g) are the adsorption ability at equilibrium and maximum. C_e (mg/L) is the concentration of dyes at equilibrium. k_L (L/mg) is the Langmuir constant while k_F (mg/g) represents the adsorption capacity. n is an empirical parameter. $q_{D\text{-}R}$ (mg/g) also represent the maximum adsorption capacity (mol/g) in D-R model, k_D is the D-R constant (mol^2/J^2) and $\varepsilon = RT\ln(1 + 1/C_e)$ is the Polanyi potential (J/mol). The values of mean free energy E (kJ/mol) are calculated by the equation 11. Besides, A_T (L/mg) and b_T (J/mol) stands for Temkin constant.

$$E = \frac{1}{\sqrt{2k_{D-R}}} \tag{11}$$

The summary of the linear fitting results for three models, Langmuir, Freundlich, and Temkin, was shown in Table 1 and Fig. S3. The order of fitting results is

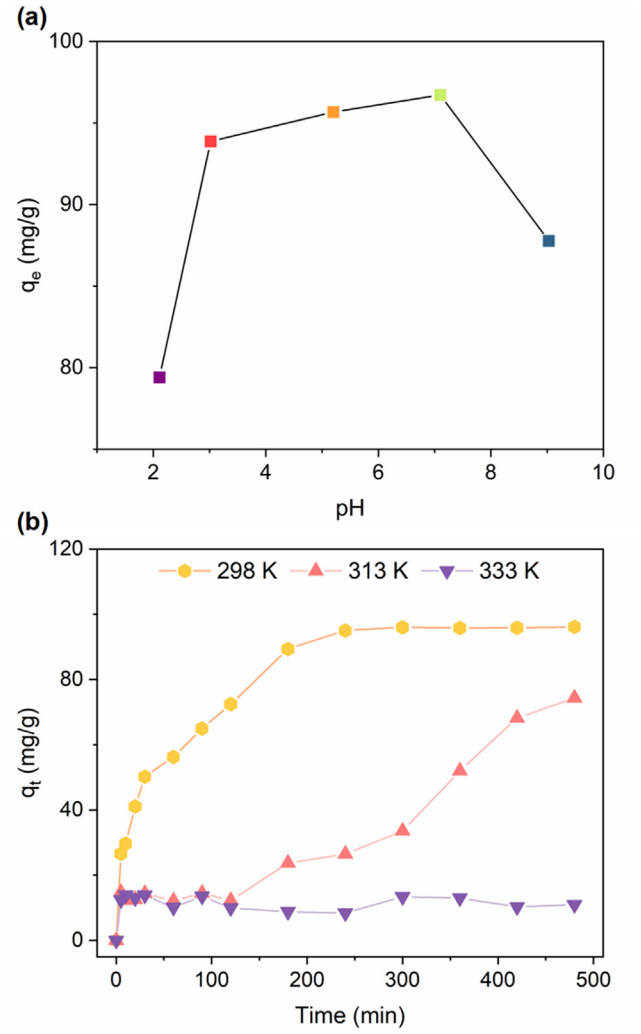

Fig. 4 (a) Effect of pH on the adsorption capacity of MB using the RCTMA@NBC. (b) Effect of temperature on the adsorption ability of MB using the RCTMA@NBC.

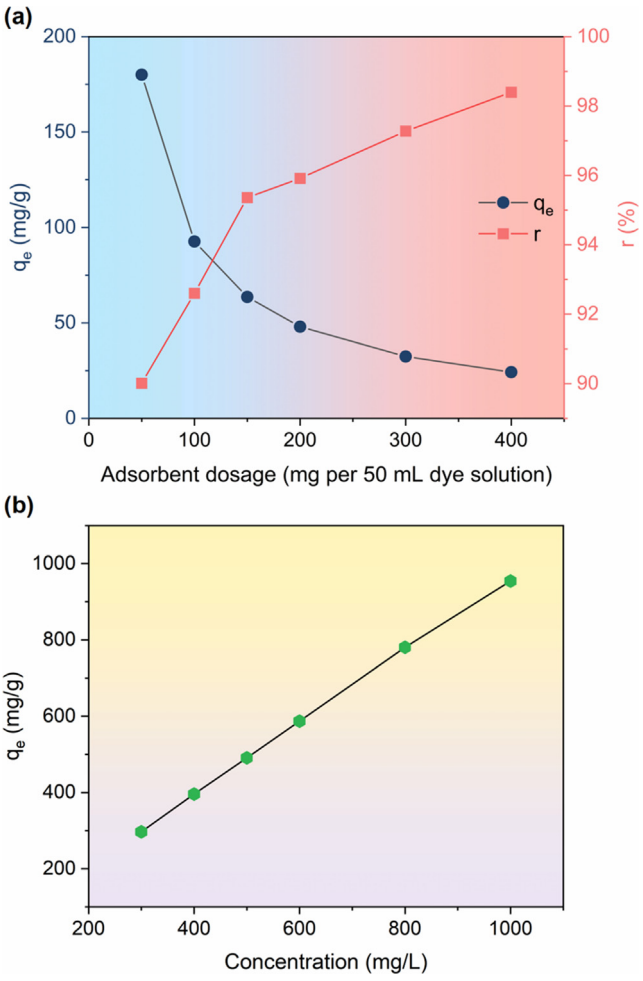

Fig. 5 (a) Effect of RCTMA@NBC's dosage on the MB adsorption. (b) Effect of dyes' concentration on the MB adsorption using the RCTMA@NBC.

Langmuir > Freundlich > Temkin > D-R. The MB adsorption using the RCTMA@NBC adsorbent is more confirmed to Langmuir model with the higher correlation coefficient (R^2) at 0.9870, compared to other models with the R^2 lower than 0.9720. According to the Langmuir isotherm model which is described the monolayer adsorption on homogeneous sites, the adsorption process of MB molecules is a monolayer adsorption onto the surface of RCTMA@NBC and the adsorption sites have the same energy. (Xie et al., 2021) The maximum adsorption capacities of MB by RCTMA@NBC was calculated as 1162.12 mg/g. The Freundlich isotherm model is used to explain the heterogeneous system with non-uniform sites and n > 1 means the adsorbent is favorable to adsorption. When the adsorption heat in the adsorption layer reduces linearly rather than exponentially with the coverage area, the Temkin isotherm model can be used to depict the adsorbent process and the value of b^T is positively proved the adsorption of MB on RCTMA@NBC is an endothermic process. The D-R model makes it possible to determine the type of adsorption as chemical or physical. The calculated E is 17.3553 KJ/mol that is > 16.0 KJ/mol which means the adsorption of MB on RCTMA@NBC is a chemical type. (Özcan et al., 2005) However, the Freundlich model, Temkin model, and D-R model are inappropriate for RCTMA@NBC due to the lower R^2.

Table 1 Isotherm constants and values of MB adsorption using the RCTMA@NBC membrane.

Model	Parameters	Value
Langmuir	q_m (mg/g)	1162.12
	k_L (L/mg)	0.0974
	R^2	0.9870
Freundlich	k_F (mg/g)	195.6008
	n	2.3113
	R^2	0.9720
Dubnin-Radushkevich (D-R)	$k_{D\text{-}R}$ (mol^2/KJ^2)	0.001660
	$q_{D\text{-}R}$	899.8607
	E (KJ/mol)	17.3553
	R^2	0.9175
Temkin	A_T (L/mg)	1.2492
	b_T (J/mol)	10.0553
	R^2	0.9698

3.4. Effect of contact time and adsorption kinetics analysis for cationic dyes

The variation of absorption capacity of MB dyes versus contact time was also investigated to the absorption kinetics. As can be seen in Fig. 6a, the trend of adsorption curve shows a convex type. The extent of adsorption exceeds quickly 200 mg/g in 5 min and the value increased over 600 mg/g as the time goes up to 180 min. When the time is further prolonged to 300 mg/g, the adsorbing capacity reaches the maximum of 726.76 mg/g and thereafter exhibits a stable plateau even increasing the contact time to 480 min. The adsorption kinetics was assessed *via* three usual models, namely pseudo-first-order, pseudo-second-order and intraparticle diffusion models which displayed in Supplementary materials SM-3. Fig. 6b-d demonstrate the fitting results depend on these three models and the kinetic parameters were aggregated in Table 2. The adsorption of MB using RCTMA@NBC is more conformed to quasi-second-order kinetic equation (R^2 = 0.9925) in comparison with pseudo-first-order and intraparticle diffusion models. The calculated adsorption equilibrium is 793.65 mg/g and this value shows an acceptable superiority than that reported by most studies summarized in Table 3. This result indicates that RCTMA@NBC adsorb the MB molecules affected by chemical adsorption *via* the positive and negative charges bonding between $COOH^-$ from RCTMA@NBC and $-C{=}N^+$ from MB dyes.

3.5. The mechanism of RCTMA@NBC's distinct adsorption behaviors

In order to determine the distinct adsorption behaviors of RCTMA@NBC, the adsorption performance of RCTMA@NBC composite adsorbent towards distinct dyes, namely cationic golden XGL and anionic brilliant crocein, are also examined. From the Fig. 7, the cationic golden XGL exhibits the similar tendency of removal rate which experiences a rapid ascend process in 60 min and thereafter a flattened to reach a plateau. The equilibrium adsorption capacity is approximate to that of MB group due to the cationic type structure (Table 2). On the contrary, the curve of brilliant crocein does not emerge the climbing state even after the time elapses 480 min. The removal efficiency values of brilliant crocein consistently hover between 3 % and 7 %, showing an irregular trend. The pseudo-first-order, pseudo-second-order and intraparticle diffusion models were used to evaluate their kinetics behaviors (Fig. S4 and Table 2). As the cationic golden XGL, the adsorption process is more consistent with the quasi-second-order kinetic equation with the higher R^2 of 0.9970 and the calculated adsorption equilibrium is 740.74 mg/g which is

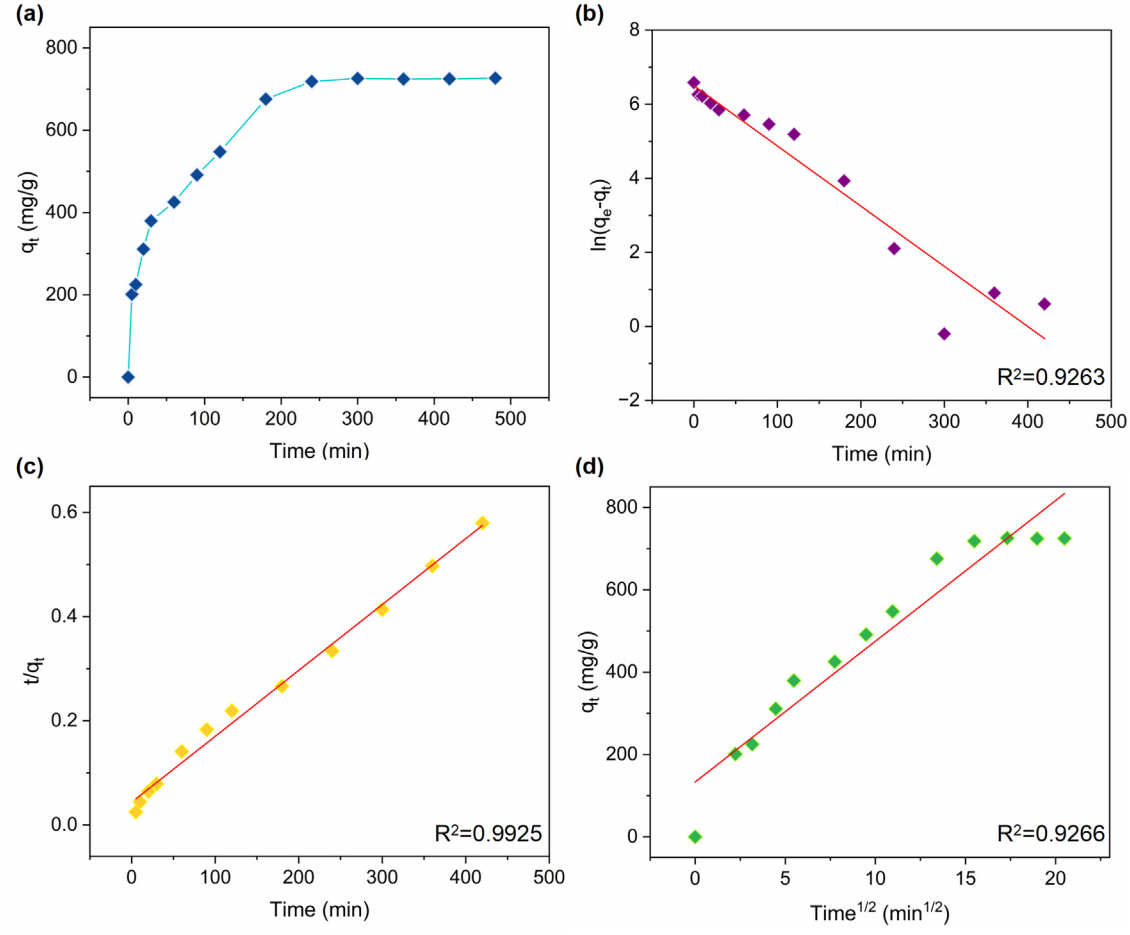

Fig. 6 (a) Effect of contact time on the MB adsorption using the RCTMA@NBC membrane. (b) Pseudo-first-order, (c) pseudo-second-order, and (d) intraparticle model of MB adsorption using the RCTMA@NBC.

Table 2 Kinetic constants and values of MB, cationic golden XGL and brilliant crocein using the RCTMA@NBC.

Model	Parameters	Value		
		MB	Cationic golden XGL	Brilliant crocein
Pseudo-first-order	$q_{e,cal}$ (mg/g)	664.00	495.29	9.34
	k_1 (min^{-1})	0.0163	0.0150	0.0022
	R^2	0.9263	0.9556	0.0593
Pseudo-second-order	$q_{e,cal}$ (mg/g)	793.65	740.74	34.26
	k_2 (g/mg·min)	0.00003627	0.00004600	−0.004799
	R^2	0.9925	0.9970	0.8886
Intraparticle	k_i ($g/mg \cdot min^{1/2}$)	34.1923	33.7921	0.2553
	C	133.1794	122.3980	34.4127
	R^2	0.9266	0.8563	0.0134

Table 3 Comparative absorptive removal of cationic MB dyes by reported adsorbents.

Cationic dyes	Adsorbents	Temperature (K)	pH	Adsorption capacity q_m (mg/g)	Adsorption kinetics	Adsorption isotherm	Mechanism of adsorption	References
MB	Cu-BTC@AG	303	7	282.466	Pseudo second-order model	Langmuir model	Electrostatic interaction	(Fu et al., 2022)
MB	Cu-Fe_3O_4@MBC	298	6 ± 0.1	156.373	Pseudo second-order model	Freundlich model	Electrostatic interaction, synergistic	(Xie et al., 2021)
MB	Cu-BTC@Algal	303	7	162.1	Pseudo second-order model	Langmuir model	Electrostatic interaction, π-π interaction	(Abdelhameed et al., 2020)
MB	AC/Cu-BTC	298	–	114.94	Pseudo second-order model	Langmuir model	Electrostatic interaction	(Liu et al., 2020)
MB	GO-CS@$Cu_3(btc)_2$	298	7	357.15	Pseudo second-order model	Langmuir model	Electrostatic interaction	(Samuel et al., 2020)
MB	CuBTC/ZnO chitosan composite	298	7	50.07	Pseudo second-order model	Langmuir model	Electrostatic interaction	(Dindorkar et al., 2022)
MB	$CuFe_2O_4$@polysaccharide	200	8	366.6	Pseudo second-order model	Langmuir model	Electrostatic interaction	(Beyki et al., 2017)
MB	BC-GO@Fe_3O_4	318	7	125	Pseudo second-order model	Freundlich model	Electrostatic interaction	(Tara et al., 2020)
MB	MnO_2/BC	318	7	185.185	Pseudo second-order model	Freundlich model	Hydrogen bonding, electrostatic interaction	(Siddiqui et al., 2019)
MB	ANFs/BC-1	303	–	59.84	Pseudo second-order	Langmuir model	Electrostatic interaction, π-π stacking interaction	(Yi et al., 2021)
MB	$CoFe_2O_4$/GO	298	7	355.9	Pseudo second-order	Langmuir model	Electrostatic interaction, π-π stacking interaction	(Chang et al., 2020)
MB	PVP/rGO/CFO	298	–	333.3	Pseudo second-order	Langmuir model	Synergistic effect of π-π conjugation interactions and electrostatic interaction	(Du et al., 2022)

(*continued on next page*)

Table 3 (*continued*)

Cationic dyes	Adsorbents	Temperature (K)	pH	Adsorption capacity q_m (mg/g)	Adsorption kinetics	Adsorption isotherm	Mechanism of adsorption	References
MB	Fe_3O_4@SiO_2@CS-TETA-GO	313	10	529.1	Pseudo second-order	Langmuir model	π-π stacking, hydrogen bonding, electrostatic interaction	(Wang et al., 2017)
MB	Fe_3O_4@PDA@UIO-66-NH-tar Fe_3O_4@PDA@UIO-66-NH-citr	313	11	381.7 432.9	Pseudo second-order	Langmuir model	Electrostatic interaction, π-π stacking and hydrogen bonding (depend on the pH)	(Fu et al., 2022)
MB	PAM/AMS/APT	298	> 5	703.3	Pseudo second-order	Langmuir model	Hydrogen bonding, electrostatic interaction	(Duan et al., 2023)
MB	RCTMA@NBC	298	7.1	1162.12	Pseudo second-order	Langmuir model	Electrostatic interaction, π-π interaction, H bonding	this study

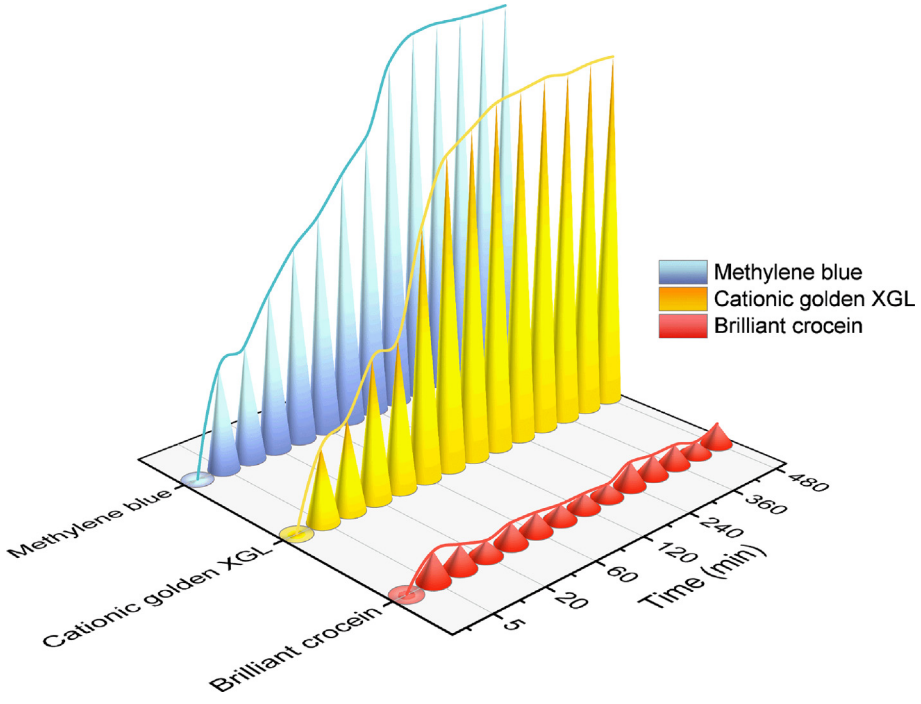

Fig. 7 The removal efficiency of MB, cationic golden XGL, and brilliant crocein using the RCTMA@NBC at different time intervals.

near the value of MB group. However, the fitting results of brilliant crocein adsorption *via* three kinds of models are not suitable due to the low R^2 smaller than 0.9000.

Obviously, the synthesized RCTMA@NBC demonstrated the selectional affinity towards cationic MB as well as cationic golden XGL, and poor adsorption efficiency to the anionic brilliant crocein. The desirable differences are mainly due to the positive and negative charge interactions between the functional groups of the adsorbent and the targeted dyes. After the RCTMA assembled into NBC, the surface of RCTMA@NBC was functionalized with abundant carboxyl groups which present the negative COO^- when they ionized in aqueous solutions

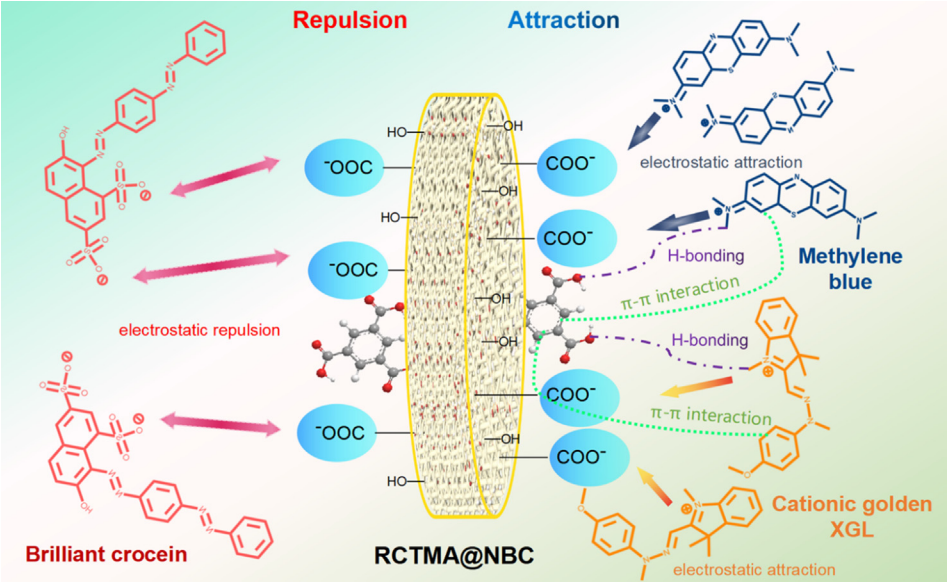

Fig. 8 The possible adsorption mechanism of RCTMA@NBC towards cationic MB and golden XGL, as well as anionic brilliant crocein dyes.

(Fig. 8). Superior hydrophilic NBC with staggered porous morphology by thin fibers is beneficial to allow dyes to gather on the surface of the adsorbent. The molecules of MB, thereby, facilely enter into the NBC and access to the nucleophilic RCTMA@NBC to form a strong binding force *via* electrostatic interaction. Mutual attraction between opposite charges is the main reason for the high adsorption phenomenon. Besides, π–π interactions and H-bonding interactions as well as the physical adsorption of NBC play a positive role in the adsorption of MB dyes. (Wang et al., 2017; Fu et al., 2022; Mantasha et al., 2020) The same behavioral pattern can be also observed in the cationic golden XGL group and the whole adsorption process is primarily affected by chemical force which has a good agreement with adsorption kinetics. Similar molecular structure makes them possess an approximate treatment ability of dyeing wastewater. On the other hand, the anion natural of brilliant crocein could be far away from the RCTMA@NBC material based on the electrostatic repulsion between the sulfonic groups from dyes and carboxy groups from adsorbent, even a certain adsorption occurred at the beginning. Therefore, the adsorption capacity of synthesized RCTMA@NBC towards cationic dyes is significantly superior to anionic dyes, which exhibits the promising potential in the field of precise treatment of organic dye wastewater.

4. Conclusion

Supramolecular TMA based hexamer, namely RCTMA that produced *via* hydrothermal method, was assembled into the porous NBC to form the RCTMA@NBC. This composite possess the three dimension crosslinked network structure and carboxyl surface functionalization, which was further employed to adsorb the cationic MB dyes by adjusting the factors like pH, temperature, and dosage of adsorbent. The experimental result showed that the maximal adsorption capacity of RCTMA@NBC appeared under the neutral environment (pH = 7.1) and the higher temperature hindered the adsorption of MB dyes. Moreover, the removal rate of MB dyes was promoted to reach nearly 99 % as the adsorbent dosage raised. Based on the adsorption isotherm analysis, it was more confirmed to Langmuir model with the higher R^2, and the maximum adsorption capacities of MB was calculated as 1162.12 mg/g. The adsorption kinetics fitting indicated the adsorption of MB using RCTMA@NBC was conformed to quasi-second-order kinetic equation, which was assigned to the chemical adsorption. More importantly, RCTMA@NBC demonstrated excellent the affinity towards cationic golden XGL based on the chemical force originated from mutual attraction between opposite charges, π–π interactions, H-bonding, as well as adsorption of the porous structure, and poor adsorption behaviour for anionic brilliant crocein was due to the electrostatic repulsion between the sulfonic groups from dyes and carboxy groups from adsorbent. This synthesized RCTMA@NBC exhibits the promising potential in the field of precise treatment of organic dyes from industrial wastewater.

Declaration of Competing Interest

The authors declare that they have no known competing financial interests or personal relationships that could have appeared to influence the work reported in this paper.

Acknowledgement

Dr. Xin Huang thanks the supporting from "The 2021 Scientific Research and Entrepreneurial Start-Ups Foundation for the Returned Overseas Chinese Scholars, Henan Province". Dr. Haijuan Du and Dr. Shaobo Wang thank "Henan Collaborative Innovation Centre of Textile and Garment Industry" and "Program for Interdisciplinary Direction Team in Zhongyuan University of Technology" for their assistance. Dr. Xin Huang appreciates the support by Henan Province Foundation for University Key Teacher (grant number 2021GGJS107), Henan Province Medical Science and Technology Project (grant number SBGJ202102185), Program for Innovative Research Team (in Science and Technology) in University of Henan Province (23IRTSTHN019), and

Strength Improvement Program for Dominant Disciplines of Zhongyuan University of Technology (grant number GG202214).

Appendix A. Supplementary material

Supplementary data to this article can be found online at https://doi.org/10.1016/j.arabjc.2023.104714.

References

Abdelhameed, R.M., Alzahrani, E., Shaltout, A.A., Moghazy, R.M., 2020. Development of biological macroalgae lignins using copper based metal-organic framework for selective adsorption of cationic dye from mixed dyes. Int. J. Biol. Macromol. 165, 2984–2993. https://doi.org/10.1016/j.ijbiomac.2020.10.157.

Ali, I., 2012. New generation adsorbents for water treatment. Chem. Rev. 112, 5073–5091. https://doi.org/10.1021/cr300133d.

Beyki, M.H., Ganjbakhsh, S.E., Minaeian, S., Shemirani, F., 2017. Clean approach to synthesis of graphene like $CuFe_2O_4$@polysaccharide resin nanohybrid: bifunctional compound for dye adsorption and bacterial capturing. Carbohydr. Polym. 174, 128–136. https://doi.org/10.1016/j.carbpol.2017.06.056.

Cao, H., Wang, R., Dou, K., Qiu, J., Peng, C., Tsidaeva, N., Wang, W., 2023. High-efficiency adsorption removal of CR and MG dyes using AlOOH fibers embedded with porous $CoFe_2O_4$ nanoparticles. Environ. Res. 216,. https://doi.org/10.1016/j.envres.2022.114730 114730.

Cazón, P., Vázquez, M., 2021. Bacterial cellulose as a biodegradable food packaging material: a review. Food Hydrocolloids 113,. https://doi.org/10.1016/j.foodhyd.2020.106530 106530.

Chang, S., Zhang, Q., Lu, Y., Wu, S., Wang, W., 2020. High-efficiency and selective adsorption of organic pollutants by magnetic $CoFe_2O_4$/graphene oxide adsorbents: experimental and molecular dynamics simulation study. Sep. Purif. Technol. 238,. https://doi.org/10.1016/j.seppur.2019.116400 116400.

Conde-González, J.E., Peña-Méndez, E.M., Melián-Fernández, A.M., Havel, J., Salvadó, V., 2021. Synthesis, performance and mechanism of nanoporous Fe-(1,3,5-tricarboxylic acid) metal-organic framework in the removal of anionic dyes from water. Environ. Nanotechnol., Monit. Manage. 16,. https://doi.org/10.1016/j.enmm.2021.100541 100541.

Das, R., Lindström, T., Sharma, P.R., Chi, K., Hsiao, B.S., 2022. Nanocellulose for sustainable water purification. Chem. Rev. 122, 8936–9031. https://doi.org/10.1021/acs.chemrev.1c00683.

Dindorkar, S.S., Patel, R.V., Yadav, A., 2022. Adsorptive removal of methylene blue dye from aqueous streams using photocatalytic CuBTC/ZnO chitosan composites. Water Sci. Technol. 85, 2748–2760. https://doi.org/10.2166/wst.2022.142.

Dou, K., Peng, C., Wang, R., Cao, H., Yao, C., Qiu, J., Liu, J., Tsidaeva, N., Wang, W., 2023. S-scheme tubular g-C_3N_4/BiOI heterojunctions for boosting photodegradation of tetracycline and Cr(VI): Mechanism insight, degradation pathway and DFT calculation. Chem. Eng. J. 455,. https://doi.org/10.1016/j.cej.2022.140813 140813.

Du, R., Cao, H., Wang, G., Dou, K., Tsidaeva, N., Wang, W., 2022. PVP modified rGO/$CoFe_2O_4$ magnetic adsorbents with a unique sandwich structure and superior adsorption performance for anionic and cationic dyes. Sep. Purif. Technol. 286,. https://doi.org/10.1016/j.seppur.2022.120484 120484.

Du, H., Wang, Z., Chen, Y., Liu, Y., Liu, Y., Li, B., Wang, X., Cao, H., 2015. Anchoring superparamagnetic core–shells onto reduced graphene oxide: fabrication of Ni–carbon–rGO nanocomposite for effective adsorption and separation. RSC Adv. 5, 10033–10039. https://doi.org/10.1039/C4RA14651D.

Duan, F., Zhu, Y., Lu, Y., Xu, J., Wang, A., 2023. Fabrication porous adsorbents templated from aqueous foams using astragalus membranaceus and attapulgite as stabilizer for efficient removal of cationic dyes. J. Environ. Sci. 127, 855–865. https://doi.org/10.1016/j.jes.2022.08.004.

Duchamp, D.J., Marsh, R.E., 1969. The crystal structure of trimesic acid (benzene-1,3,5-tricarboxylic acid). Acta Crystallogr. Sect. B: Struct. Sci. 25, 5–19. https://doi.org/10.1107/S0567740869001713.

Fu, Q.P., Shi, D.H., Mo, C.L., Lou, J., Zhou, S.Q., Zha, L., Wang, J. L., Yan, W., Luo, J., 2022. Adsorption behavior of methylene blue on regenerable composite Cu-BTC@AG. J. Solid State Chem. 311,. https://doi.org/10.1016/j.jssc.2022.123100 123100.

Fu, Y., Xu, Y., Lou, B., Qin, X., Zhang, L., Yuan, H., Zhang, L., Zhang, Y., Lu, J., 2022. Magnetically recyclable core–shell MOF nanoparticles of Fe_3O_4@PDA@UIO-66-NH_2 grafted by organic acids for intensified cationic dye adsorption. New J. Chem. 46, 11071–11081. https://doi.org/10.1039/D2NJ01748B.

Han, T., Zheng, J., Han, Y., Xu, X., Li, M., Schwarz, C., Zhu, L., 2021. Comprehensive insights into core microbial assemblages in activated sludge exposed to textile-dyeing wastewater stress. Sci. Total Environ. 791,. https://doi.org/10.1016/j.scitotenv.2021.148145 148145.

Hirani, R.A.K., Asif, A.H., Rafique, N., Wu, H., Shi, L., Zhang, S., Duan, X., Wang, S., Saunders, M., Sun, H., 2022. Three-dimensional nitrogen-doped graphene oxide beads for catalytic degradation of aqueous pollutants. Chem. Eng. J. 446,. https://doi.org/10.1016/j.cej.2022.137042 137042.

Hu, K., Liu, Z.R., Xiu, T.Y., Zhou, L.M., Wang, Y., 2020. Removal of thorium from aqueous solution by adsorption with $Cu_3(BTC)_2$. J. Radioanal. Nucl. Chem. 326, 185–192. https://doi.org/10.1007/s10967-020-07310-6.

Huang, X., Li, B., Wang, S., Yue, X., Zhengguo, Y., Deng, X., Ma, J., 2020. Facile in-situ synthesis of PEI-Pt modified bacterial cellulose bio-adsorbent and its distinctly selective adsorption of anionic dyes. Colloids Surf., A 586,. https://doi.org/10.1016/j.colsurfa.2019.124163 124163.

Huang, C., Liao, H., Ma, X., Xiao, M., Liu, X., Gong, S., Shu, X., Zhou, X., 2021. Adsorption performance of chitosan Schiff base towards anionic dyes: electrostatic interaction effects. Chem. Phys. Lett. 780,. https://doi.org/10.1016/j.cplett.2021.138958 138958.

Liu, Z., Fan, A., Ho, C.-H., 2020. Preparation of AC/Cu-BTC composite and its adsorption mechanisms. J. Environ. Eng. 146,. https://doi.org/10.1061/(ASCE)EE.1943-7870.0001678 123100.

Lv, P., Yao, Y., Li, D., Zhou, H., Naeem, M.A., Feng, Q., Huang, J., Cai, Y., Wei, Q., 2017. Self-assembly of nitrogen-doped carbon dots anchored on bacterial cellulose and their application in iron ion detection. Carbohyd. Polym. 172, 93–101. https://doi.org/10.1016/j.carbpol.2017.04.086.

Mantasha, I., Saleh, H., Qasem, K., Shahid, M., Ahmad, M., 2020. Efficient and selective adsorption and separation of methylene blue (MB) from mixture of dyes in aqueous environment employing a Cu(II) based metal organic framework. Inorg. Chim. Acta. https://doi.org/10.1016/j.ica.2020.119787 119787.

Nidheesh, P.V., Zhou, M., Oturan, M.A., 2018. An overview on the removal of synthetic dyes from water by electrochemical advanced oxidation processes. Chemosphere 197, 210–227. https://doi.org/10.1016/j.chemosphere.2017.12.195.

Özcan, A.S., Erdem, B., Özcan, A., 2005. Adsorption of Acid Blue 193 from aqueous solutions onto BTMA-bentonite. Colloids Surf., A 266, 73–81. https://doi.org/10.1016/j.colsurfa.2005.06.001.

Qiu, B.Y., Gorgojo, P., Fan, X.L., 2022. Adsorption desalination: advances in porous adsorbents. Chin. J. Chem. Eng. 42, 151–169. https://doi.org/10.1016/j.cjche.2021.08.032.

Rajkumar, M., Muthuraja, P., Dhandapani, M., Chandramohan, A., 2020. Synthesis, crystal structure, optical, thermal, mechanical, dielectric and DFT studies of 3, 5-dimethylprazole:1,3,5-benzene tricarboxylic acid molecular adduct crystal. Opt. Laser Technol. 124,. https://doi.org/10.1016/j.optlastec.2019.105970 105970.

Rivera-Utrilla, J., Sánchez-Polo, M., Gómez-Serrano, V., Álvarez, P. M., Alvim-Ferraz, M.C.M., Dias, J.M., 2011. Activated carbon modifications to enhance its water treatment applications. an overview. J. Hazard. Mater. 187, 1–23. https://doi.org/10.1016/j.jhazmat.2011.01.033.

Samsami, S., Mohamadizaniani, M., Sarrafzadeh, M.-H., Rene, E.R., Firoozbahr, M., 2020. Recent advances in the treatment of dye-containing wastewater from textile industries: overview and perspectives. Process Saf. Environ. 143, 138–163. https://doi.org/10.1016/j.psep.2020.05.034.

Samuel, M.S., Suman, S., Venkateshkannan, Selvarajan, E., Mathimani, T., Pugazhendhi, A., 2020. Immobilization of $Cu_3(btc)_2$ on graphene oxide-chitosan hybrid composite for the adsorption and photocatalytic degradation of methylene blue. J. Photochem. Photobiol., B 204. https://doi.org/10.1016/j.jphotobiol.2020.111809.

Siddiqui, S.I., Manzoor, O., Mohsin, M., Chaudhry, S.A., 2019. Nigella sativa seed based nanocomposite-MnO_2/BC: an antibacterial material for photocatalytic degradation, and adsorptive removal of Methylene blue from water. Environ. Res. 171, 328–340. https://doi.org/10.1016/j.envres.2018.11.044.

Tang, J., Yamauchi, Y., 2016. MOF morphologies in control. Nat. Chem. 8, 638–639. https://doi.org/10.1038/nchem.2548.

Tara, N., Siddiqui, S.I., Nirala, R.K., Abdulla, N.K., Chaudhry, S.A., 2020. Synthesis of antibacterial, antioxidant and magnetic Nigella sativa-graphene oxide based nanocomposite BC-GO@Fe_3O_4 for water treatment. Colloid Interface Sci. Commun. 37,. https://doi.org/10.1016/j.colcom.2020.100281 100281.

Tokoh, C., Takabe, K., Fujita, M., Saiki, H., 1998. Cellulose synthesized by acetobacter xylinum in the presence of acetyl glucomannan. Cellulose 5, 249–261. https://doi.org/10.1023/A:1009211927183.

Uddin, M.J., Ampiaw, R.E., Lee, W., 2021. Adsorptive removal of dyes from wastewater using a metal-organic framework: a review. Chemosphere 284,. https://doi.org/10.1016/j.chemosphere.2021.131314 131314.

Wang, C., Kim, J., Tang, J., Kim, M., Lim, H., Malgras, V., You, J., Xu, Q., Li, J., Yamauchi, Y., 2020. New strategies for novel MOF-derived carbon materials based on nanoarchitectures. Chem 6, 19–40. https://doi.org/10.1016/j.chempr.2019.09.005.

Wang, S., Peng, Y., 2010. Natural zeolites as effective adsorbents in water and wastewater treatment. Chem. Eng. J. 156, 11–24. https://doi.org/10.1016/j.cej.2009.10.029.

Wang, F., Zhang, L., Wang, Y., Liu, X., Rohani, S., Lu, J., 2017. Fe_3O_4@SiO_2@CS-TETA functionalized graphene oxide for the adsorption of methylene blue (MB) and Cu(II). Appl. Surf. Sci. 420, 970–981. https://doi.org/10.1016/j.apsusc.2017.05.179.

Xia, Z., Zhao, Y., Darling, S.B., 2021. Covalent organic frameworks for water treatment. Adv. Mater. Interfaces 8, 2001507. https://doi.org/10.1002/admi.202001507.

Xie, J., Lin, R., Liang, Z., Zhao, Z., Yang, C., Cui, F., 2021. Effect of cations on the enhanced adsorption of cationic dye in Fe_3O_4-loaded biochar and mechanism. J. Environ. Chem. Eng. 9,. https://doi.org/10.1016/j.jece.2021.105744 105744.

Yaghi, O.M., Li, H.L., Groy, T.L., 1996. Construction of porous solids from hydrogen-bonded metal complex of 1,3,5 benzenetricarboxylic acid. J. Am. Chem. Soc. 118, 9096–9101.

Yan, M., Huang, W., Li, Z., 2019. Chitosan cross-linked graphene oxide/lignosulfonate composite aerogel for enhanced adsorption of methylene blue in water. Int. J. Biol. Macromol. 136, 927–935. https://doi.org/10.1016/j.ijbiomac.2019.06.144.

Yi, X., Wang, F., Wu, Y., He, J., Huang, Y., 2021. Aramid nanofibers/bacterial cellulose nanocomposite aerogels for high-efficient cationic dye removal. Mater. Chem. Phys. 272,. https://doi.org/10.1016/j.matchemphys.2021.124985 124985.

Yin, N., Chen, S., Li, Z., Ouyang, Y., Hu, W., Tang, L., Zhang, W., Zhou, B., Yang, J., Xu, Q., Wang, H., 2012. Porous bacterial cellulose prepared by a facile surfactant-assisted foaming method in azodicarbonamide-NaOH aqueous solution. Mater. Lett. 81, 131–134. https://doi.org/10.1016/j.matlet.2012.04.133.

Zou, X., Zhang, H., Chen, T., Li, H., Meng, C., Xia, Y., Guo, J., 2019. Preparation and characterization of polyacrylamide/sodium alginate microspheres and its adsorption of MB dye. Colloids Surf. A 567, 184–192. https://doi.org/10.1016/j.colsurfa.2018.12.019.